Korean J. Chem. Eng., 33(5), 1590-1598 (2016)
DOI: 10.1007/s11814-015-0282-9

pISSN: 0256-1115
eISSN: 1975-7220

Fundamental study of $LaMg_xCr_{1-x}O_{3-\delta}$ perovskites nano-photocatalysts: Sol-gel synthesis, characterization and humidity sensing

Benjamin Avila Josephine[*,], Ayyar Manikandan[***,†], Vincent Mary Teresita[*,**], and Susaimanickam Arul Antony[*,****,†]**

*Research and Development Center, Bharathiar University, Coimbatore - 641046, India
**Department of Chemistry, Stella Maris College, Chennai - 600 086, India
***Department of Chemistry, Bharath Institute of Higher Education and Research, Bharath University, Chennai - 600 073, India
****PG and Research Department of Chemistry, Presidency College (Autonomous), Chennai - 600 005, India
(*Received 5 September 2015 • accepted 11 December 2015*)

Abstract−Nanocrystalline perovskite oxides, $LaMg_xCr_{1-x}O_{3-\delta}$ (x=0.0, 0.2, 0.4, 0.6, 0.8 and 1) were prepared by sol-gel method. The samples were characterized by powder X-ray diffraction (XRD), scanning electron microscopy (SEM), Fourier transform infrared (FT-IR) spectroscopy and nitrogen adsorption/desorption isotherms at 77 K, respectively, to identify the structural phases, surface morphology, vibrational stretching frequencies and BET surface area of the samples. Also, it was investigated the humidity sensing characteristics of the samples. The composites were sintered at 800 °C for 5 h and subjected to dc electrical conductivity studies at room temperature. The resistance measurements as a function of relative humidity (RH) in the range of 5-98% were done and the humidity sensing factors ($S_f = R_{5\%}/R_{98\%}$) calculated. The activation energy of the compounds were determined from the temperature-dependent electrical conductance experiments in the temperature range of 120-300 °C. LaMgCr-3 (x=0.4) had the highest humidity sensing factor 21407±431, while LaCr-1 (x=0) the lowest sensitivity factor 27.27±2. The response and recovery characteristics were studied for LaMgCr-3, which exhibited good linearity and a very narrow hysteresis loop. The photocatalytic activity of $LaMg_xCr_{1-x}O_{3-\delta}$ was investigated by using the photo-decomposition of 4-chlorophenol (4-CP) under UV-visible light. The sample LaMgCr-3 (x=0.4) showed the highest photocatalytic degradation efficiency (93.05%) than other samples, due to their smaller size of particles with higher surface area.

Keywords: Sol-gel Method, Perovskites Oxides, Humidity Sensors, Ceramics, Catalyst

INTRODUCTION

The measurement and control of humidity is important in many areas, including meteorology, domestic environment, medicine, food production, industry and agriculture. The development of humidity sensors that are inexpensive, highly sensitive and selective is still in progress. Desirable characteristics of humidity sensors are high sensitivity over a wide humidity range, quick response time, stability, resistance to contaminants, insignificant dependence on temperature, simple structure, low cost, good thermal and chemical stability [1,2]. A wide variety of materials have been studied as sensing elements in humidity sensors and used for commercial devices. New humidity sensing materials for a wide range of applications in various fields have been synthesized over the years. The materials used in humidity sensors exploiting variations of electrical parameters are roughly classified into three groups: electrolytes, organic polymers and ceramics. Ceramic materials have shown advantages in terms of their mechanical strength, resistance to chemical attack and thermal and physical stability. Ceramic materials have received much attention due to their chemical inertness in recent years. Different ceramic materials have been studied as humidity sensors [3].

Chakoumakos et al. [4] suggested that strontium aluminate possessed increased reactivity spontaneously with water forming a range of complex hydroxides. Vijaya et al. [5] reported strontium-copper-aluminum mixed metal oxide spinel composites by a sol-gel method for humidity sensing application. Kipyung et al. [6] used spinel magnesium aluminate nanostructures for humidity sensing. Laobuthee et al. [7] repoted spinel magnesium aluminate prepared by oxide one pot synthesis (OOPS) for humidity sensing. Stambolova et al. [8] and Arshak et al. [9] reported the potential of several novel semiconducting materials as viable gas-sensing materials. Jung et al. [10] reported carbon-nitride films with ~20 nm grain size on Si substrate for applying to integrated humidity sensors. Rajmohan et al. [11] reported $La_{1-x}Ni_xVO_3$ composites were prepared by coprecipitation method for humidity sensing. Katoch et al. [12] reported Pt nanoparticle-decorated networked ZnO nanowire for room temperature gas sensors.

Among the different types of humidity sensors, the metal oxides and mixed metal oxides are more promising, due to their high physical and chemical stability. Many metal oxides containing transition and rare earth metal ions have been studied for humidity sensing properties. They are the most versatile solid state sensors.

†To whom correspondence should be addressed.
E-mail: mkavath15@gmail.com, manikandana.che@bharathuniv.ac.in, antonypresidency15@gmail.com

Extensive research work has been carried out over the years to study the electrical conductivity, transport properties and the effect of doping on the humidity sensing properties of many mixed metal oxides. The combination of two metals in an oxide matrix can produce materials with novel structural or electronic properties that can lead to superior performance in technological applications. Materials based on metal chromites have long been identified as a possible active material in chemical sensing applications. Lanthanum chromites possess thermal and chemical stability and relatively high electrical conductivity; they are also doped with other metals to enhance the electrical conductivity, and this has proved to be useful for its sensing properties [13-15].

In recent years, nanostructured semiconductor based photocatalysts have attracted much attention for dye degradation. The present study is focused on the degradation of 4-chlorophenol (4-CP), due to the aromatic ring and chlorine atom, existence acute toxicity, which results in negative effects including carcinogenicity [16,17]. Our research group has used spinel ferrites and metal sulfides for the degradation of 4-CP [16-19]. Among various semiconductors, $LaMg_xCr_{1-x}O_{3-\delta}$ based materials are the well known photocatalysts, which are under extensive research for breakdown of organic based impurities. Sol-gel method has been used to synthesize $LaMg_xCr_{1-x}O_{3-\delta}$ nano-photocatalysts to work under UV-Visible light. This method is selected because it cheap, facile and economical.

In the present investigation, novel nanocrystalline perovskite oxides, $LaMg_xCr_{1-x}O_{3-\delta}$ (x=0.0, 0.2, 0.4, 0.6, 0.8 and 1) prepared by sol-gel method were characterized by powder X-ray diffraction, scanning electron microscopy (SEM), FT-IR spectroscopy and nitrogen adsorption/desorption isotherms at 77 K, respectively, to identify the structural phases, surface morphology, vibrational stretching frequencies and BET surface area of the compounds. The compounds were investigated for humidity sensing characteristics. The effect of adsorbed water on the electrical conductance of the compounds and the dependence of electrical response of these oxide pellets on the relative humidity was studied. The results show that they can be proposed as materials for humidity sensing.

EXPERIMENTAL

1. Sample Preparation

The nanocrystalline $LaMg_xCr_{1-x}O_{3-\delta}$ oxides were prepared by sol-gel method using $La(NO_3)_3{\cdot}6H_2O$, $Mg(NO_3)_2$, $Cr(NO_3)_3{\cdot}9H_2O$ (AR grade >98%) as starting materials. Different mole ratios of these metal nitrates (Table 1) of analytical grade were dissolved in deionized water, and citric acid was added as the gelling agent. The citric acid was dissolved in ethylene glycol at 100 °C. The resulting solution was stirred at room temperature until a clear transparent solution was obtained. This clear solution was kept for gellation at 100 °C for 12 h and the gel was then dried at 150 °C followed by calcination at 600 °C for 5 h. The calcined powders were ground and made in the form of cylindrical pellets of dimension 13 mm diameter and 3-4 mm thickness using a hydraulic press at a pressure of 400 MPa. The pellets were then sintered at 800 °C for 5 hrs in ambient air atmosphere. The samples were cooled to room temperature at the natural cooling rate of the furnace.

Table 1. Different mole ratios of $LaMg_xCr_{1-x}O_{3-\delta}$

Sample code	$La(NO_3)_3$ (moles)	$Cr(NO_3)_3$ (moles)	$Mg(NO_3)_2$ (moles)
LaCr-1	1	1	0
LaMgCr-2	1	0.8	0.2
LaMgCr-3	1	0.6	0.4
LaMgCr-4	1	0.4	0.6
LaMgCr-5	1	0.2	0.8
LaMg-6	1	0	1

2. Characterization Methods and Humidity Sensing Studies

Structural studies were carried out using Bruker AXS D8 Advance diffractometer for 2θ values ranging from 0 to 80° using CuKα radiation at λ=1.5406 Å. The crystallite size D was calculated using the Debye-Scherrer formula [20,21].

$$D = \frac{0.89\lambda}{\beta\cos\theta} \quad (1)$$

where λ is the wavelength of the incident X-ray (λ=1.54 Å), β is the full width half maximum (FWHM) in radians of the maximum intensity peak and θ is the angle at which the maximum peak occurs.

The Fourier transform infrared (FT-IR) spectra were recorded with Perkin - Elmer spectrometer using KBr pellets whose thickness was about 1.3 mm. Each spectrum was collected at room temperature under atmospheric pressure. The samples were dispersed in spectroscopic grade KBr pellets and were scanned in the range of 4,000-400 cm^{-1}.

The surface morphology of the sintered porous compounds was studied with Ultra 55 FESEM analyzer operating at the desired magnification. A gold coating was deposited on the sample to avoid charging of the surface.

The dc electrical resistance at relative humidity levels for the samples in the form of pellets using conducting silver paste to ensure ohmic contacts was determined by a two-probe method, and the changes in the surface conductivity as a function of applied field and current were measured [22]. The electrical contact was made on the surface of the pellet by means of two thin copper wires affixed with silver paint. The samples were electrically connected to a dc power supply and a Keithley 6485 picoammeter in series.

The controlled humidity environments were achieved using anhydrous P_2O_5, saturated aqueous solutions of $CaCl_2{\cdot}6H_2O$, $Ca(NO_3)_2{\cdot}4H_2O$, NH_4Cl and $CuSO_4{\cdot}5H_2O$ in a closed glass vessel at an ambient temperature of 25 °C, which yielded approximately 5, 31, 51, 79, 98% relative humidity, respectively [23]. Heat cleaning of the samples was found to be a must for a better sensitivity. Hence the samples were heated to 100 °C for 2 h, followed by cooling in a humidity-free atmosphere before and after the sensitivity measurements, especially when the sensors were operated at higher RH. The samples were exposed to the respective percentage of RH until the saturation reached around 2h.The sensitivity factor S_f was calculated by the ratio of resistances $R_{5\%}/R_{98\%}$, where $R_{5\%}$ and $R_{98\%}$ were the dc resistances, at 5 and 98 RH%, respectively. The temperature-dependent conductance experiments in the temperature range of 120-300 °C under ambient conditions were carried out to

determine the activation energies of the samples using the linearized form of the expression,

$$I=Io\ exp^{-Ea/kT} \quad (2)$$

where, I is the current, Ea the activation energy, k the Boltzmann constant and T the temperature. For this purpose the pellets were kept inside a cylindrical furnace that was connected to microprocessor controlled temperature programmer.

A degassed glass chamber (200 cm^3) was used for the evaluation of response and recovery characteristics. This chamber has a provision for a two-way inlet, one for transpiring dry air from 5% RH and the other for transpiring moist air from 98% RH. The response and recovery characteristics were studied between 5 and 98% RH conditions. The resistance measurements in dry air as well as in moist air alternatively helped to establish the recovery and response characteristics for moisture sensing, and the stability of the sensing material was also monitored for 30-48 days.

3. Photocatalytic Reactor Setup and Degradation Procedure

All photochemical reactions under identical conditions were carried out in a self-designed photocatalytic reactor. This model consists of eight medium pressure mercury vapor lamps (8 W) set in parallel and emitting 365 nm wavelength. It has a reaction chamber with specially designed reflectors made of highly polished aluminum and built-in cooling fan at the bottom and black cover to prevent UV leakage. It is provided with the magnetic stirrer at the center. Open borosilicate glass tube of 40 cm height and 12.6 mm diameter was used as a reaction vessel. The irradiation was carried out using only six parallel medium pressure mercury lamps. The solution was aerated continuously by a pump to provide oxygen and for the complete mixing of solution. Prior to photocatalytic experiments, the adsorption of 4-CP on $LaMg_xCr_{1-x}O_{3-\delta}$ nano photo-catalyst was carried out by mixing 100 ml of aqueous solution of 4-CP with fixed weight of the respective photo-catalyst. All solutions prior to photolysis were kept in dark by covering with aluminum foil to prevent any photochemical reactions.

RESULTS AND DISCUSSION

1. Powder XRD Studies

The powder XRD patterns (Fig. 1) correspond to LaCr-1, LaMgCr-2 to5 and LaMg-6 compounds. The average crystallite size of all the samples estimated by Debye Scherrer formula was found to be 51.75, 32.06, 9.83, 14.34, 22.80 and 35.12 nm for LaCr-1, LaMgCr-2, LaMgCr-3, LaMgCr-4, LaMgCr-5 and LaMg-6, respectively. The ionic radius of Mg^{2+} ions (0.86 Å) was higher than Cr^{3+} ions (0.755 Å). As the number of moles of Mg^{2+} ions increases in

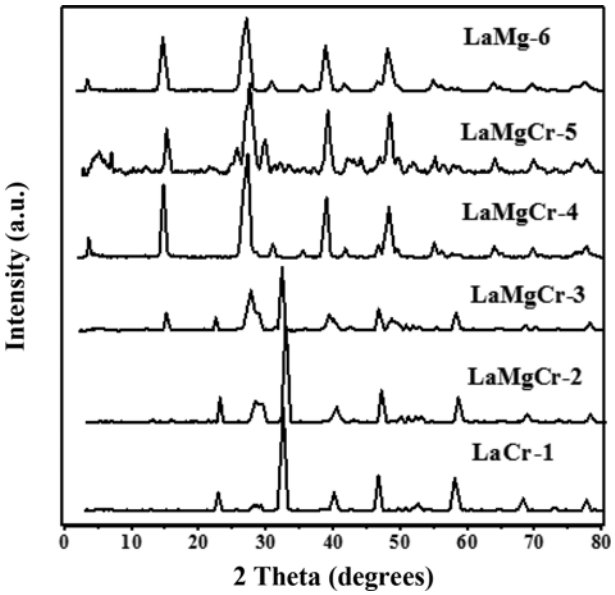

Fig. 1. Powder XRD pattern of $LaMg_xCr_{1-x}O_{3-\delta}$.

$LaCrO_3$ system, the crystallite size increases or decreases depending upon whether the Mg^{2+} ions completely fit into the "B" site of the perovskite structure. One of the most important criteria for a good humidity sensor material is that the crystallite size must be small, which will support the mobility of the dominant charge carriers. Thus, the ionic conductivity of the compound will increase. On comparing the crystallite size of LaMgCr-2 to LaMgCr-5 compounds, LaMgCr-3 has the smallest crystallite size in which 0.4 moles of Cr^{3+} ions are replaced by 0.4 moles of Mg^{2+} ions in the perovskite structure. This is one evidence for LaMgCr-3 to be a high sensing material in the $LaMg_xCr_{1-x}O_{3-\delta}$ series of compounds.

The d-spacing values of $LaCrO_3$ (LaCr-1) compounds matched with JCPDS No. 83-1327 show the orthorhombic crystalline ABO_3 perovskite type phase. The 2θ values with (*hkl*) planes at 22.86° (*011*), 32.66° (*002*), 40.26° (*202*), 46.78° (*400*), 58.22° (*402*) and 77.63° (*233*) for $LaCrO_3$ were observed. All the diffraction peaks can be indexed as a pure orthorhombic perovskite structure. The strong and sharp peaks indicate good crystallinity in $LaCrO_3$.

The XRD pattern of LaMgCr-2 to 6 does not match exactly with any of the existing XRD patterns. The XRD patterns of LaMgCr-2 to LaMgCr-6 compounds were analyzed and found to be an orthorhombic system with a defined space group which is shown in Table 2 [24-28]. These reports have been deposited in International Centre for Diffraction Data (ICDD). XRD analysis also shows a

Table 2. XRD analysis of nanocrystalline perovskite compounds

Sample code	Crystal system	a (Å)	b (Å)	c (Å)	Unit cell volume ($Å^3$)	Space groups
$LaMg_{0.2}Cr_{0.8}O_{3-\delta}$ [24]	Orthorhombic	5.501	7.754	5.473	233.4	Pnma
$LaMg_{0.4}Cr_{0.6}O_{3-\delta}$ [25]	Orthorhombic	5.492	7.737	5.474	232.6	Pnma
$LaMg_{0.6}Cr_{0.4}O_{3-\delta}$ [26]	Orthorhombic	8.701	14.952	8.687	1130.2	Abm2
$LaMg_{0.8}Cr_{0.2}O_{3-\delta}$ [27]	Orthorhombic	8.680	14.942	8.670	1124.5	Abm2
$LaMgO_{3-\delta}$ [28]	Orthorhombic	8.661	14.934	8.589	1110.8	Abm2

gradual increase in unit cell volume from LaMgCr-2 to 6 compounds, which is due to the replacement of Cr^{3+} with Mg^{2+} ions in the B site of the perovskite structure. The XRD analysis acts as tool in explaining the humidity sensing nature of the compound under humidity sensing measurements.

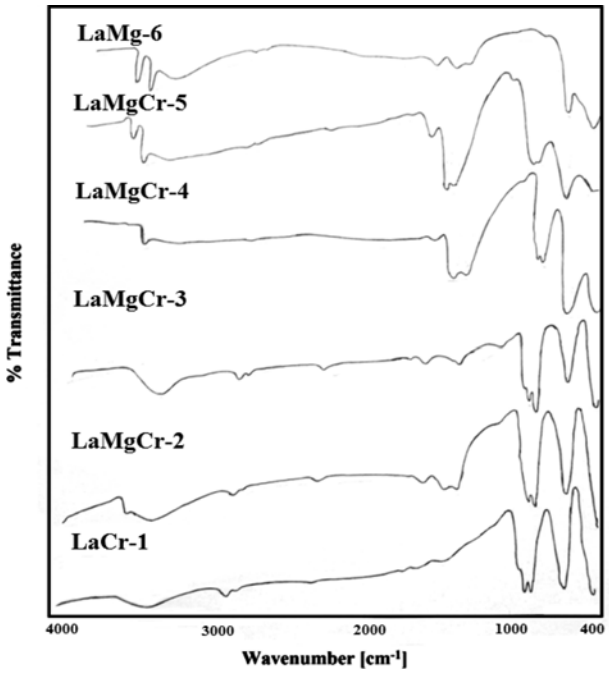

Fig. 2. FT-IR spectra of $LaMg_xCr_{1-x}O_{3-\delta}$.

2. FT-IR Spectroscopy

The FT-IR spectra of LaCr-1, LaMgCr-2 to LaMgCr-5 and LaMg-6 nanocrystalline compounds (Fig. 2) exhibit a common band near 3,400 cm^{-1} due to the OH- stretching vibrations of free and hydrogen-bonded hydroxyl groups, and a second typical absorption region at 1,630 cm^{-1} is assigned to the deformative formation of water molecules, which is most probably due to water adsorption during the compaction of the powder specimens with KBr. The metal-oxygen stretching frequencies in the range 400-1,000 cm^{-1} are associated with vibrations of La-O, Cr-O and Mg-O bonds present in the compounds.

3. SEM Analysis

The SEM micrograph images of nanocrystalline perovskites LaCr-1, LaMgCr-3, LaMgCr-4 and LaMg-6 qualitatively depict intragranular porous structure and are shown in (Fig. 3(a)-(d)). The particle size of lanthanum chromites (LaCr-1) and lanthanum magnesium oxide (LaMg-6) is in the range of 100 nm and 1 μm with less porosity. The particle size of LaMgCr-3 is around 100 nm, which shows a well defined grain size with high porosity. On comparison of the SEM micrographs, LaMgCr-3 shows larger grain size and decrease in particle size than that of LaCr-1, LaMgCr-4 and LaMg-6. LaMgCr-3 shows a well developed porosity which plays a very important role in humidity sensing studies. Thus, high

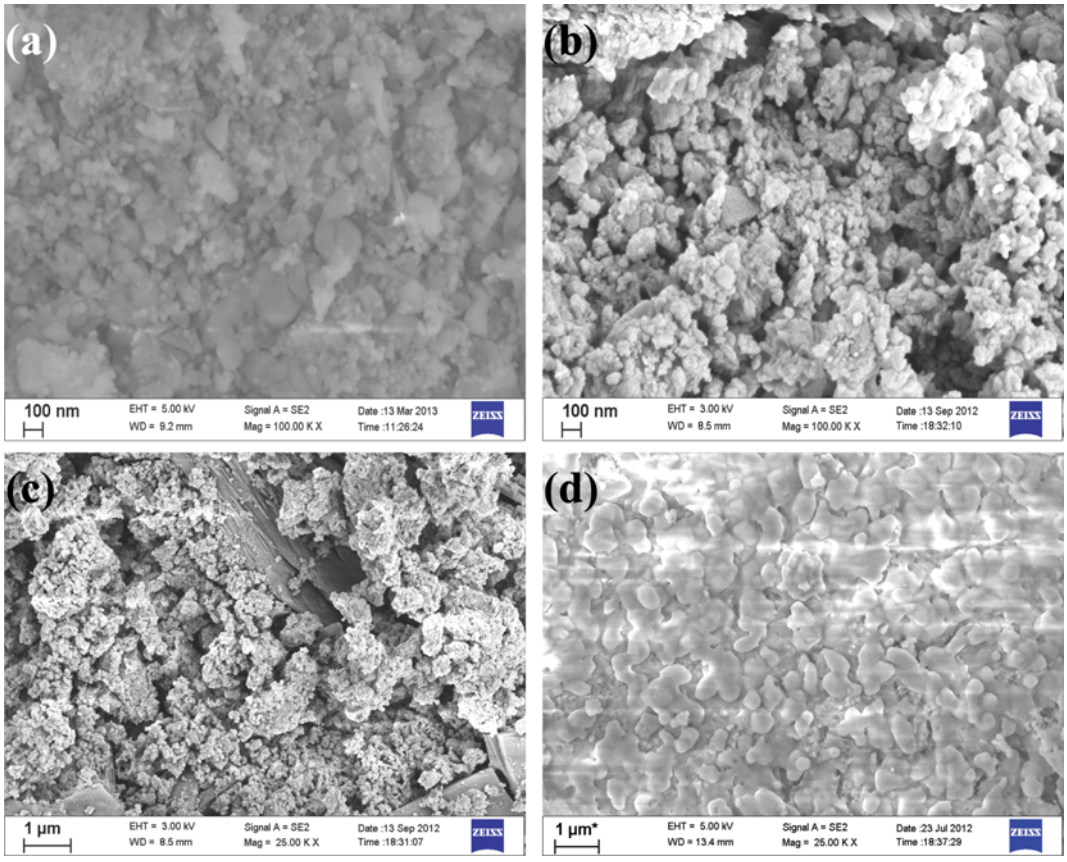

Fig. 3. SEM micrographs of (a) LaCr-1, (b) LaMgCr-3, (c) LaMgCr-4 and (d) LaMg-6.

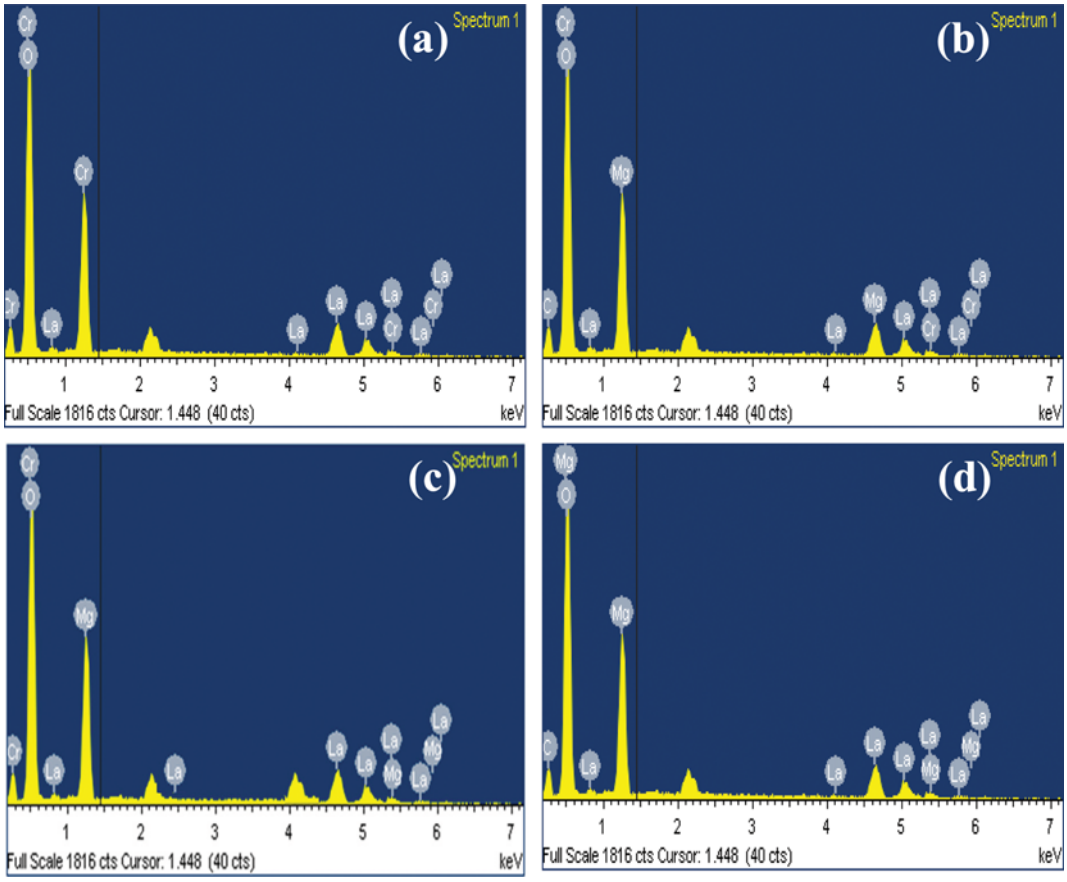

Fig. 4. EDX spectra of (a) LaCr-1, (b) LaMgCr-3, (c) LaMgCr-4 and (d) LaMg-6.

sensing property of $LaMg_{0.4}Cr_{0.6}O_{3-\delta}$ (LaMgCr-3) is supported by the SEM micrographs.

4. EDX Analysis

The EDAX spectra of LaCr-1, LaMgCr-3, LaMgCr-4 and LaMg-6 are also shown in Fig. 4(a)-(d). LaCr-1 spectra Fig. 4(a) confirms the atomic ratio of La, Cr and O (1 : 1 : 3) agrees with the standard stoichiometric composition. Fig. 3(d) shows the presence of La, Mg and O in LaMg-6 compound. Fig. 4(b), (c) confirms the existence of lanthanum, chromium, magnesium and oxygen present in the precursor of LaMgCr-3 and LaMgCr-4. There are no impurities observed, which suggests high purity of the compounds.

5. Temperature Dependent Studies

The electrical conductance measurements that were taken for nanocrystalline lanthanum magnesium chromite ($LaMg_xCr_{1-x}O_{3-\delta}$) compounds (Fig. 5), at room temperature, prior to relative humidity measurements signified that the current increased linearly with the applied voltage, indicating the ohmic contact of the electrodes. The temperature dependence of electrical conductance study carried out in the 100-300 °C range suggested that the current (I) increased with an increase in temperature (T). The applied voltage was 10V. The activation energy was calculated from the temperature dependent electrical conductance data using Arrhenius equation and is shown in Table 3. The activation energy for electrical conduction in polycrystalline materials generally involves the combination of the energy required to raise the carriers from the dominant levels to their corresponding transport bands and the energy required to create the charge carriers in the dominant levels [29]. The low activation energy of LaMgCr-3 (0.047 eV) compound predicts that the small polaron conduction dominates in the studied temperature range.

6. Humidity Measurements

The results of the resistance measurements as a function of RH at a fixed ambient temperature of 25 °C are shown in Fig. 6. The ohmic nature of the electrode contact was ascertained from the linear dependence of the measured current with applied field (2-30 V) at constant temperature. For a better appreciation of the material characteristics towards moisture, the sensitivity factor (S_f)=$R_{5\%}/R_{98\%}$, where $R_{5\%}$ and $R_{98\%}$ are the dc resistances at 5% and 98% RH, respectively, were evaluated in Table 3. This ratio is referred to as the sensitivity factor, S_f. The greater the value of $R_{5\%}/R_{98\%}$ (that is, lesser the resistance or more conductance at $R_{98\%}$), the higher the sensitivity of the material towards moisture [29]. The resistance of the compounds changes depending upon the porosity of the material. As the porosity of the nanocrystalline compound increases, the adsorption and capillary condensation of water on the surface of the compound increases, which increases the humidity level in the compound.

Good linearity in the plot of log R vs RH% is shown in Fig. 6; it is an important criterion for good humidity sensitivity material.

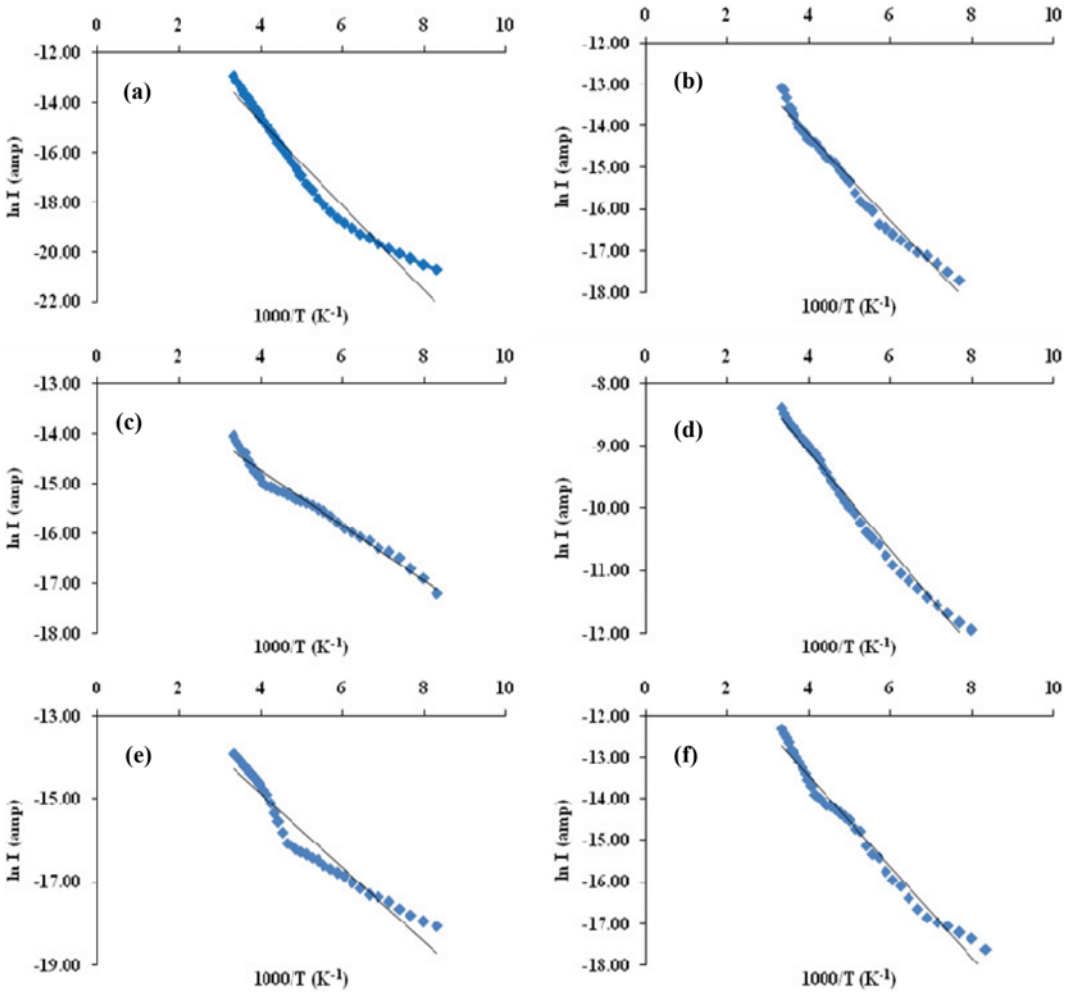

Fig. 5. Temperature dependence of electrical conductance for $LaMg_xCr_{1-x}O_{3-\delta}$ compounds (a) LaCr-1, (b) LaMgCr-2, (c) LaMgCr-3, (d) LaMgCr-4, (e) LaMgCr-5 and (f) LaMg-6.

Table 3. Humidity response and physical characteristics of perovskite compounds

S. no.	Sample code	Resistance (ohms) of relative humidity (RH%)		Sensitivity factor	Ea	BET surface
		$R_{5\%}$	$R_{98\%}$	$S_f=R_{5\%}/R_{98\%}$	(eV)	area (m^2/g)
1	LaCr-1	7.9825×10^{7}	2.9268×10^{6}	27.27±2	0.271	3.95
2	LaMgCr-2	1.2587×10^{10}	8.5291×10^{6}	1475.77±54	0.088	8.42
3	LaMgCr-3	3.5281×10^{10}	1.6481×10^{6}	21407.07±431	0.047	29.71
4	LaMgCr-4	7.2837×10^{10}	8.6243×10^{6}	8445.56±169	0.067	18.41
5	LaMgCr-5	2.3845×10^{10}	3.8641×10^{6}	6170.91±124	0.076	14.46
6	LaMg-6	3.9670×10^{11}	5.2846×10^{8}	750.67±23	0.094	7.13

Among the different nanocrystalline lanthanum magnesium chromites LaMgCr-3 shows good sensing ability towards humidity, which contains 0.4 mole of Mg^{2+} and 0.6 mole of Cr^{3+}. LaCr-1 and LaMg-6, though they show a linear trend, the drop in resistances with increases in RH value is very small and cannot be used as the humidity sensors. Chemisorption takes place at low humidity levels, leading to the formation of free hydroxyl on the surface with the charge transport occurring by the hopping mechanism [20]. On comparing the substituted chromite compounds, that is, LaMgCr-2 to LaMgCr-5, LaMgCr-3 experiences a drop in resistance in the entire range of RH, which makes it the best sensing compound with S_f value of 21,407.07±431; this is due to the water being physisorbed on the top of the chemisorbed layer. As a result, the condensation of water in the capillary-like pores leads a liquid-like layer leading to electrolytic conduction. It is further supported by SEM image photographs which show an increase in porosity of LaMgCr-3 compound. The sensitivity factor of nanocrystalline lanthanum magnesium chromites $LaMg_xCr_{1-x}O_{3-\delta}$ is shown in Table

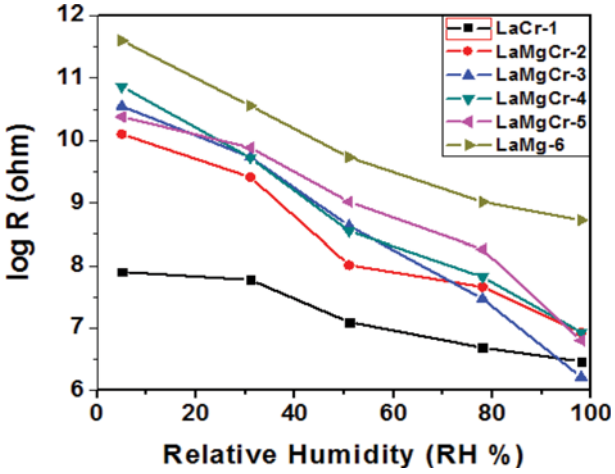

Fig. 6. Plot of log R vs RH% of nanocrystalline lanthanum magnesium chromites.

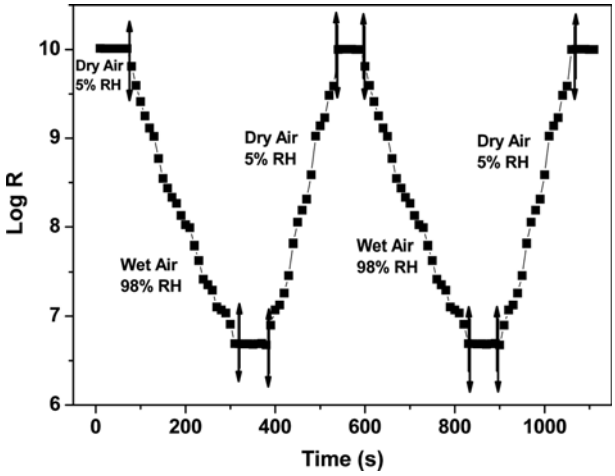

Fig. 7. Response and recovery time characteristic of LaMgCr-3 compound between 5 and 98%.

3. The maximum sensitivity shown by LaMgCr-3 in the series of lanthanum magnesium chromites is because Mg^{2+} ions contain electrostatically bonded water and form a continuous hydrogen-bonded network throughout the solid state lattice. The surface structure of water molecules can change the conductance and increase the sensitivity factor. Thus, Mg^{2+} along with the presence of lanthanum chromite moiety in LaMgCr-3 (0.4 moles of Mg^{2+} and 0.6 moles of Cr^{3+}) increases the sensitivity factor towards humidity.

7. Response, Recovery and Stability Characteristics

As LaMgCr-3 was proved to be a good sensing material, the response and recovery measurements were performed. A degassed chamber was used for keeping the sensor to exposure to dry (5% RH) and moist air (98% RH) alternatively at a constant of 10 V. The change in resistance in the presence of dry air and moist air was used to measure the response and recovery properties of the sensor material. The response and recovery characteristics of LaMgCr-3 are shown in Fig. 7. The resistance is on the order of $10^{10}\ \Omega$ drops down to a constant value of $10^{6}\ \Omega$ The response and recovery time of the sensor material was 240 s and 160 s. The response time was found to be higher than the recovery time. The water molecule adsorbed on the surface of the material due to purging of moist air was swept off by the alternate dry air in 160s. The response and recovery studies were repeated for five cycles to check the reproducibility of the results. The good sensitivity, response and recovery characteristics are another evidence for LaMgCr-3 to be a good sensing material in the presence of moist air. The response and recovery curve of the LaMgCr-3 compound was further supported by the stability of the compound, which was obtained by plotting R (ohms) vs Days. From Fig. 8, there was not much variation in the resistance, even after studying the sample after 30 to 48 days duration. This accounts for the stability of the LaMgCr-3 compound.

8. Photocatalytic Properties

The PCD efficiency of $LaMg_xCr_{1-x}O_{3-\delta}$ samples is shown in

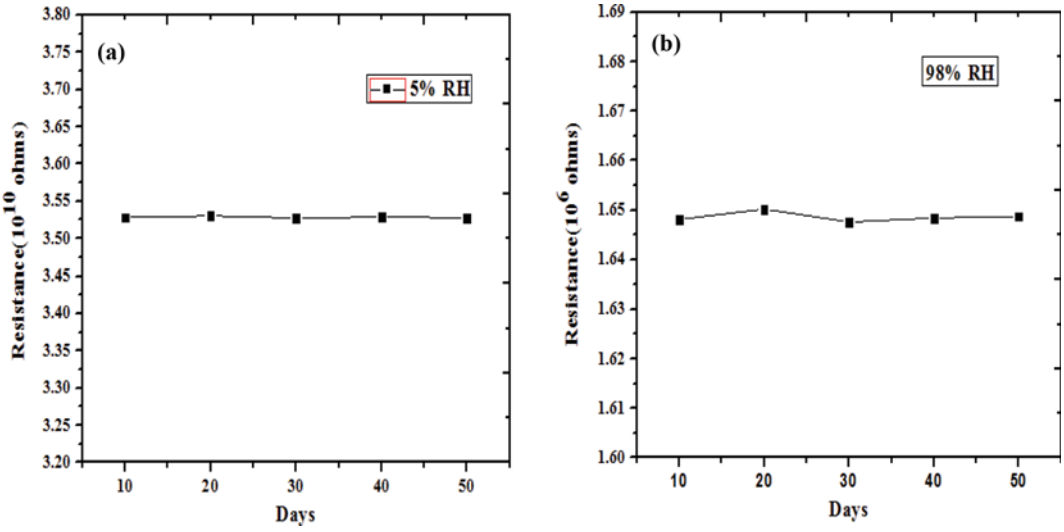

Fig. 8. Stability curve for humidity sensing studies of LaMgCr-3 compound at 5 and 98% RH.

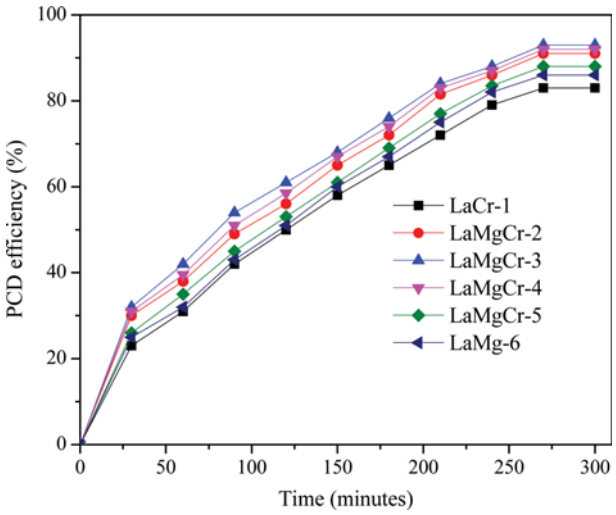

Fig. 9. Effect of Mg doping on the PCD efficiency of $LaMg_xCr_{1-x}O_{3-\delta}$ photocatalyst (conditions: 4-CP=200 mg/L, photocatalyst= 30 mg/100 mL, k=365 nm).

Fig. 9. The PCD efficiency of LaCr-1 is very low when compared with other compositions. The PCD efficiency of LaMgCr-3 is higher than LaCr-1 and LaMg-6. However, the PCD efficiency of $LaMg_xCr_{1-x}O_{3-\delta}$ increased with an increase in the concentration of Mg loading and showed maximum activity at x=0.4 (LaMgCr-3). It is mainly due to the smaller particle size distribution of LaMgCr-3 and higher surface area. Therefore, the improvement in the PCD efficiency of $LaMg_xCr_{1-x}O_{3-\delta}$ as Mg doping increases was recognized as the small particle size and higher defect application.

This is further confirmed and supported by BET surface adsorption studies shown in Table 3. On comparing the surface area of the nanocrystalline $LaMg_xCr_{1-x}O_{3-\delta}$ compounds LaMgCr-3 shows a high surface area value 29.71 m^2/g. Therefore, it is believed that the high surface area of LaMgCr-3 could enhance the photocatalytic activity than other samples (Fig. 8). In general, a high specific surface area has a favorable effect on the activity for photo-catalysts. Thus, the higher surface area of the sample LaMgCr-3 may lead to higher photocatalytic degradation efficiency (93.05%) than other samples [30-32]. In addition, the amount of the dispersion of particles per volume in the solution will increase, resulting in the enhancement of the photon absorbance [33-35].

CONCLUSIONS

Nanocrystalline perovskite oxides having different mole ratios of $LaMg_xCr_{1-x}O_{3-\delta}$ were fabricated and studied for humidity sensing applications. As the drop in resistance of LaCr-1 and LaMg-6 was less compared to the other compounds, these were not very promising. The compound $LaMg_{0.4}Cr_{0.6}O_{3-\delta}$ (LaMgCr-3) was found to be a good humidity sensor among the compounds with the sensitivity factor of 21,407.07±431, which was further evidenced by BET surface areas, E_a values and SEM images showing porous structures of the compound. The better response and recovery characteristic at room temperature was another proof for a good humidity sensor and could be promising material in future for wide applications. The as-prepared crystalline $LaMg_xCr_{1-x}O_{3-\delta}$ exhibited photodegradation of 4-CP under UV-Visible light and the sample LaMgCr-3 showed higher photocatalytic degradation efficiency (93.05%) than other samples.

ACKNOWLEDGEMENT

The authors would like to thank Dr. Fr. Jeyaraj SJ former Principal of Loyola College, Dr. Selvanayagam former director of Loyola Institute of Frontier Energy (LIFE) and Dr. Sr. Jasintha Quadras *f.m.m*, Principal, Stella Maris College, for giving permission to use instruments and other facilities.

REFERENCES

1. Z. Chen and C. Lu, *Sens. Lett.*, **3**, 274 (2005).
2. J. J. Vijaya, L. John Kennedy, A. Meenakshisundaram, G. Sekaran and K. S. Nagaraja, *Sens. Actuators B*, **127**, 619 (2007).
3. A. M. E. Suresh Raj, C. Mallika, K. Swaminathan, O. M. Sreedharan and K. S. Nagaraja, *Sens. Actuators B*, **81**, 229 (2002).
4. B. C. Chakoumakos, G. A. Lager and J. A. Fernandez-Baca, *Acta Crystallogr. C*, **48**, 414 (1992).
5. J. J. Vijaya, L. J. Kennedy, G. Sekaran and K. S. Nagaraja, *Mater. Res. Bull.*, **43**, 473 (2008).
6. A. Kipyung, B. W. Wessels and S. Sampath, *Sens. Actuators B*, **107**, 342 (2005).
7. A. Laobuthee, S. Wongkasemjit, E. Traversa and R. M. Laine, *J. Eur. Ceram. Soc.*, **20**, 91 (2000).
8. I. Stambolova, K. Konstantinov, S. Vassilev, P. Peshev and T. Tsacheva, *Mater. Chem. Phys.*, **63**, 104 (2000).
9. K. Arshak and I. Gaiden, *Mater. Sci. Eng. B*, **118**, 44 (2005).
10. J. Jung and S. P. Lee, *J. Nanosci. Nanotechnol.*, **13**, 7030 (2013).
11. S. Rajmohan, A. Manikandan, V. Jeseentharani, S. A. Antony and J. Pragasam, *J. Nanosci. Nanotechnol.*, **16**, 1650 (2016).
12. A. Katoch, S. W. Choi, G. J. Sun and S. S. Kim, *J. Nanosci. Nanotechnol.*, **13**, 7097 (2013).
13. Y. Chen, X. Lu, Y. Ding, X. Liu and G. Meng, *J. Rare Earths*, **28**, 153 (2010).
14. L. F. G. Setz, I. Santacruz, M. T. Colomer, S. R. H. M. Castanho and R. Moreno, *Mater. Res. Bull.*, **46**, 983 (2011).
15. N. Kavasoglu and M. Bayhan, *Turk. J. Phys.*, **29**, 249 (2005).
16. A. Manikandan, M. Durka, K. Seevakan and S. Arul Antony, *J. Supercond. Nov. Magn.*, **28**, 1405 (2015).
17. A. Manikandan, M. Durka and S. Arul Antony, *J. Inorg. Organomet. Polym.*, **25**, 804 (2015).
18. A. Manikandan, M. Durka and S. Arul Antony, *Adv. Sci. Eng. Med.*, **7**, 33 (2015).
19. A. Manikandan, E. Hema, M. Durka, K. Seevakan, T. Alagesan and S. Arul Antony, *J. Supercond. Nov. Magn.*, **28**, 1783 (2015).
20. R. K. Kotnala, J. Shah, B. Singh, H. Kishan, S. Singh, S. K. Dhawan and A. Sengupta, *Sens. Actuators B*, **129**, 909 (2008).
21. K. S. Chou, T. K. Lee and F. J. Liu, *Sens. Actuators B*, **56**, 106 (1999).
22. E. S. Raj, C. Mallika, O. M. Sreedharan and K. S. Nagaraja, *Mater. Res. Bull.*, **36**, 845 (2001).
23. S. Pokheral and K. S. Nagaraja, *Sens. Actuators B*, **92**, 144 (2003).
24. D. Sornadurai, B. Josephine, V. Teresita and S. Antony, ICDD card

00-063-0472, January 13 (2014).
25. D. Sornadurai, B. Josephine, V. Teresita and S. Antony, ICDD card # 00-063-0473, January 13 (2014).
26. D. Sornadurai, B. Josephine, V. Teresita and S. Antony, ICDD card # 00-063-0474, January 13 (2014).
27. D. Sornadurai, B. Josephine, V. Teresita and S. Antony, ICDD card # 00-063-0475, January 13 (2014).
28. D. Sornadurai, B. Josephine, V. Teresita and S. Antony, ICDD card # 00-063-0492, January 13 (2014).
29. S. Pokhrel and K. S. Nagaraja, *Phy. Stat. Sol. A*, **198**, 343 (2003).
30. A. Manikandan, R. Sridhar, S. Arul Antony and S. Ramakrishna, *J. Mol. Struct*., **1076**, 188 (2014).
31. A. Manikandan, M. Durka and S. Arul Antony, *J. Supercond. Nov. Magn*., **28**, 209 (2015).
32. A. Manikandan, M. Durka and S. Arul Antony, *J. Inorg. Organomet. Polym*., **25**, 1019 (2015).
33. A. Manikandan, M. Durka and S. Arul Antony, *J. Supercond. Nov. Magn*., **27**, 2841 (2014).
34. A. Manikandan and S. Arul Antony, *J. Supercond. Nov. Magn*., **27**, 2725 (2014).
35. A. Manikandan, M. Durka and S. Arul Antony, *J. Supercond. Nov. Magn*., **28**, 2047 (2015).